Published in : Supercond. Sci. Technol (2024), vol. 37, 16pp
DOI: 10.1088/1361-6668/ad68d1
Status : Postprint (Author's version)

ENHANCING THE MAGNETIC FIELD GRADIENT BETWEEN TWO SUPERCONDUCTORS WITH ROTATIONAL MOTION UNDER A BACKGROUND DC FIELD

M Houbart[1,*], J-F Fagnard[1], P Harmeling[1], J Dular[2], A R Dennis[3], D K Namburi[4], J H Durrell[3], C Geuzaine[1], B Vanderheyden[1] and P Vanderbemden[1]

[1] *Department of Electrical Engineering and Computer Science, University of Liege, B-4000 Liege, Belgium*

[2] *TE-MPE-PE, CERN, Geneva, Switzerland*

[3] *University of Cambridge, Bulk Superconductivity Group, Cambridge CB2 1PZ, United Kingdom*

[4] *Quantum Sensors Group, James Watt School of Engineering, University of Glasgow, Glasgow G12 8QQ, United Kingdom*

E-mail: michel.houbart@uliege.be

ABSTRACT

The ability of bulk high-temperature superconductors to trap magnetic flux densities up to one order of magnitude larger than the saturation magnetization of conventional ferromagnetic materials offers the prospect of generating large magnetic flux density gradients. Combining multiple superconductors, akin to assembling a Halbach array of permanent magnets, may increase the generated gradient even further. The associated challenge is that superconductors are prone to demagnetization when exposed to field components perpendicular to their main magnetization direction. In the present work, we investigate the magnetic flux density gradient achieved with a pair of cubic, bulk, large-grain melt-textured superconductors in the presence of a background DC magnetic field at 77 K. We investigate the increase of the performance when decreasing the temperature down to 59 K. The studied configuration consists in two facing cubic $YBa_2Cu_3O_{7-x}$ superconductors of 6 mm side with anti-parallel magnetization directions. It is obtained after the simultaneous magnetization of the samples followed by a rotation of 180° of the top superconductor. Although the background field reduces the trapped field ability of individual samples, it is shown that this phenomenon is significantly mitigated at 65 K and at 59 K compared to 77 K. The results reveal that a sample-to-sample distance (~16 mm) of the order of their size is sufficient to avoid any mutual demagnetization effect during the rotational motion. Furthermore, it is shown that decreasing the temperature is not only beneficial in increasing the field and field gradient achieved but also in extending the range of background fields in which the superconductor can be rotated without demagnetization. This superconducting assembly yields a magnetic flux density gradient exceeding that of an isolated superconductor and has the potential to surpass the capabilities of permanent magnets.

* Author to whom any correspondence should be addressed.

Published in : Supercond. Sci. Technol (2024), vol. 37, 16pp
DOI: 10.1088/1361-6668/ad68d1
Status : Postprint (Author's version)

KEYWORDS: bulk superconductor, trapped-field magnet, magnetic field gradient, interacting bulk superconductors, rotating superconductor, flux pinning

1. INTRODUCTION

The force acting on a magnetic material results both from the magnitude and the gradient of the magnetic flux density. When using an assembly of permanent magnets for generating compactly such a magnetic force for magnetic drug delivery applications [1–4], the range of the force is limited by the decay of both the magnetic field strength and gradient with distance from the assembly. Considering this limitation, an attractive method has emerged, known as 'dipole field navigation' [5–8]. It involves taking advantage of the magnetic flux density gradient resulting from the insertion of a soft ferromagnetic core in a large uniform DC magnetic field. The uniform DC field is exploited to ensure full saturation magnetization of the magnetic material on which the force is acting while the soft ferromagnetic core introduces a localized distortion of the homogeneous field, thereby generating the required gradient. In this approach, however, the saturation magnetization of the soft ferromagnetic core employed limits the maximum achievable field gradient ($\mu_0 M_{sat} \sim 2.4$ T for soft ferromagnetic Fe–Co alloys [9]).

Given that superconductors are not limited by magnetic saturation [10–13], they are attractive candidates for replacing the ferromagnetic cores in dipole field navigation. This idea was recently investigated by Arsenault and Sirois [14] where the remote force produced by a superconducting disk inserted and rotated in a scanner was evaluated by numerical modelling. The use of superconductors in such applications raises several questions since their insertion and mechanical motion in the background DC magnetic field can induce an alteration of their magnetization similar to what is observed in so-called 'crossed-field' experiments [15–22]. In this context, the purpose of the present work is to investigate experimentally and numerically the magnetic flux density gradient achievable in a targeted spatial region when one or two magnetized $YBa_2Cu_3O_{7-x}$ bulk superconductors are magnetized in the presence of a DC background field and one of them is rotated so that its magnetization becomes reversed, when compared to the field. This process generates a distortion of the magnetic flux lines which produces the required gradient, either in the vicinity of a single superconductor, or in the gap between two of them.

2. EXPERIMENTAL METHODS

2.1. Superconducting samples

The measurements are conducted on two cubic $YBa_2Cu_3O_{7-x}$ bulk superconductors, each with a side length of 6 mm. These dimensions correspond to the largest samples that can be accommodated in the experimental setup developed in this work. These cubic samples were extracted from two larger cylindrical samples manufactured using the top seeded melt growth (TSMG) method [23–26] within the Bulk Superconductivity Group at the University of Cambridge. The two samples used in this work were selected from a larger batch in such a way that they exhibited highly similar superconducting properties [27].

The 6 mm side cubes were extracted from the cylindrical bulk samples using a Testbourne wire saw model 850. The tool continuously moves a 100 μm stainless steel wire forming a loop. As it moves, the wire carries an

Published in : Supercond. Sci. Technol (2024), vol. 37, 16pp
DOI: 10.1088/1361-6668/ad68d1
Status : Postprint (Author's version)

abrasive slurry which grinds against the material to be cut. The extracted portions correspond to cubic regions positioned centrally within the cylinder, each of them including the seed of the initial large grain sample. Additionally, a much smaller orthorhombic sample of dimensions 1.5×1.8×5 mm^3 was also extracted from one of the cylindrical superconductors, in a region adjoining the position of the cube. This orthorhombic sample with largest side parallel to the *c*-axis was intended for *M*(*H*) loop measurements and was assumed to exhibit superconducting properties that are very close to those of the cubic samples.

2.2. Experimental setup

Experiments were carried out in the experimental chamber of a *Physical property measurement system* (PPMS) [28]. This equipment allows measurement of several physical characteristics through a variety of insertion instruments commercialized by *Quantum Design*. The easy access to the sample chamber offers the possibility to design be spoke insertion tools aimed at exploring configurations such as the dielectric properties of insulators [29] or the magnetic properties of bulk superconductors [18, 30–33]. In this work, the PPMS was used for two distinct categories of experiments. The first category was a set of preliminary DC *M*(*H*) loop measurements conducted with the *AC measurement system* (ACMS) option of the PPMS [34]. The loops were recorded at 77 K, 65 K and 59 K, with maximum applied fields $\mu_0 H_{max}$ of 4 T, 6 T and 7 T respectively. The second category aimed to investigate the magnetic behaviour of bulk superconductors undergoing rotation within a background field at different temperatures. For this, a customized insertion tool compatible with the PPMS was designed and developed. This tool is designed to accommodate two cubic superconducting samples of 6 mm side. One of the samples is clamped and held stationary, while controlled rotational motion of the other is made possible. A picture of the final setup, as well as the superconducting samples used, is depicted in figure 1. In this figure are also shown the direction of axes employed in this work: the *z*-direction is the direction of the applied field and the *y*-direction corresponds to the axis of rotation of the rotating sample holder.

Figure 1 shows that the system includes a rack and pinion mechanism which enables a 190° rotation of a sample holder within the experimental chamber of the PPMS while counteracting a resistive torque of up to 0.022 N m. Once the samples are installed in the system, the line passing through their geometric centres is parallel to the *z*-direction and the distance between the 2 closest face is 16.6 mm. As it will become clearer in the following sections, this separation distance is sufficient to prevent mutual demagnetization, while still being small enough to justify considering a two-sample configuration rather than an isolated superconductor.

As shown in figure 1, the superconductors placed in the stationary and rotating sample holders are denoted sample 1 and sample 2 respectively. The setup is also equipped with a home-made sensing device including 13 stationary HGT-2101 Hall sensors. This sensing device is referred to as the 'Multi-Hall probe' in figure 1 and measures the magnetic flux density distribution between the superconductors, along a line passing through their geometrical centres. The design and the calibration of this bespoke probe are presented in more detail in appendix.

Published in : Supercond. Sci. Technol (2024), vol. 37, 16pp
DOI: 10.1088/1361-6668/ad68d1
Status : Postprint (Author's version)

Figure 1. Picture of the bespoke insertion instrument compatible with the PPMS. Dimensions are in mm.

2.3. Experimental procedure

The bespoke experimental system shown in figure 1 was used to investigate various configurations involving either one or two cubic superconductors at 77 K, 65 K and 59 K. While the experimental parameters for each configuration under investigation differed, a common framework is consistently used across all experiments. The experimental process consisted of three systematic steps represented schematically in figure 2 and described in more detail below.

Published in : Supercond. Sci. Technol (2024), vol. 37, 16pp
DOI: 10.1088/1361-6668/ad68d1
Status : Postprint (Author's version)

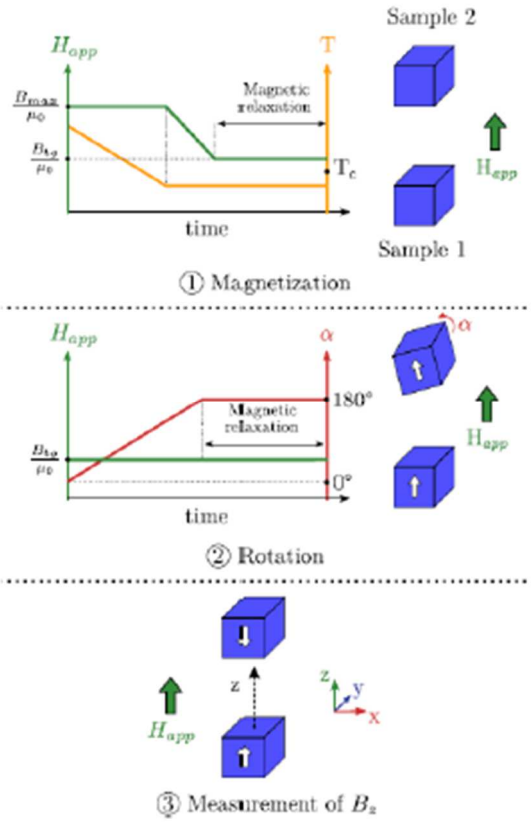

Figure 2. Schematic illustration of the systematic experimental process used during the experiments conducted in this work.

(1) The samples are magnetized either in field cooling (FC) or in zero-field-cooling (ZFC) conditions. Only the FC condition is represented schematically in figure 1. For both magnetization processes, the applied magnetic field is oriented in the *z*-direction which coincides with the alignment of the *c*-axes of the samples. The maximum applied field multiplied by μ_0 is noted B_{max} and the field sweep rate is 15 mT s^{-1}. A notable feature of this procedure is that the field-decreasing step is stopped when the applied field reaches a given background threshold denoted B_{bg}, then it remains unchanged for the rest of the experiment. A period of 45 minutes starting at the end of the field-decreasing step is allowed for magnetic relaxation.

(2) The rotating sample holder is rotated by an angle of 180° at a constant speed of 5° s^{-1}. After this rotation, a second period of 15 minutes is allowed for further magnetic relaxation. Note that this step is performed even if no sample is placed in the rotating holder so that the total magnetic relaxation period is the same for all experiments.

(3) The magnetic flux density distribution component parallel to the applied field is measured simultaneously at 13 positions between the samples using the multi-Hall probe described in appendix. Unless otherwise stated, the magnetic flux densities and gradients of magnetic flux density are measured at this specific instant. Since the applied field is aligned with the active axis of the Hall sensors, the contribution of superconducting samples is obtained by subtracting Bbg ≠0 from the measurements.

Published in : Supercond. Sci. Technol (2024), vol. 37, 16pp
DOI: 10.1088/1361-6668/ad68d1
Status : Postprint (Author's version)

Table 1. List of the experiments carried out within the PPMS.

T° [K]	Magnetization process	B_{max} [mT]	Sample	B_{bg} [mT]
77	ZFC	2400	1	0
				100
				200
				300
			2	0
				100
				200
				300
			1 + 2	0
				100
				200
				300
65	FC	4000	1	0
				50
				100
				150
			2	0
				50
				100
				150
			1 + 2	0
				50
				100
				150
59	FC	7000	1 + 2	0
				50

A comprehensive list of the experiments carried out with the bespoke instrument shown in figure 1 is presented together with their specific experimental parameters in table 1.

3. FINITE ELEMENT MODEL

A numerical tool available within the Life-HTS toolkit [35] was used to get insights into the distribution of current density within the considered superconducting assemblies. This model is based on the 3D mixed *h*-Ø-*a* formulation developed in [36]. More precisely, an *h*-formulation is employed to characterize the superconducting domains, while an *a*-formulation is applied to model the non-conductive regions. The coupling between these formulations is achieved thanks to surface terms computed on the common boundary. This numerical tool was successfully adapted in our previous work [37] to model the translational motion of superconductors and it is extended in the present work to explore the rotation of superconducting samples. The rotation is modelled through the iterative adjustment of the position of superconducting regions at discrete time intervals. The *a*-field and *h*-field calculated in the previous time step undergo suitable shifts to assess their

Published in : Supercond. Sci. Technol (2024), vol. 37, 16pp
DOI: 10.1088/1361-6668/ad68d1
Status : Postprint (Author's version)

time derivatives [38]. Note that the rotational movement induces an acceleration, which is omitted in the model. It can be shown that this approximation remains valid provided that the angular velocity of the conductor is much smaller than the electronic cyclotron frequency [39]

The superconductors modelled are perfect cubes with a side of 6 mm and are meshed with hexahedral elements of approximately 0.5 mm side length. A power law is used as electric constitutive law within the superconducting regions and the critical exponent is set to n=40, a common value for $YBa_2Cu_3O_{7-x}$ superconductors at 77 K [40, 41]. The critical current density used in the power law is assumed to be homogeneous, isotropic and to depend on the magnetic flux density according to the law proposed in [42]:

$$J_c(B) = J_{c,0}\left[\frac{1}{1+\frac{B}{B_0}} + \frac{a}{\left(\frac{B}{B_0}-b_1\right)^2+(b_2)^2}\right]. \qquad (1)$$

Equation (1) extends Kim's model by adding a Lorentzian term accounting for a potential fishtail effect. This additional term reaches its maximum value when $B/B_0 = b_1$ and the magnitude of this maximum is $a/(b_2)^2$. The parameter b_2 is defined such that the Lorentzian reaches half of its maximum value when $B/B_0 = b_1 \pm b_2$. It has been shown [42] that equation (1) is sufficiently general to parametrize a variety of fishtail effects and can be used to approximate a wide range of magnetization loop shapes.

4. RESULTS AND DISCUSSION

Section 4.1 deals with the magnetic properties of the stationary samples in order to determine the n value and the $J_c(B)$ law that will be inserted in the numerical modelling of the flux density generated by the permanently magnetized bulk superconductors. Section 4.2 investigates the flux density generated by one single bulk sample rotated in a background DC field. Section 4.3 investigates the flux density distribution between two bulk samples in a background DC field, one of which undergoing a 180° rotation.

4.1. Characterization of a single stationary sample

4.1.1. Flux creep analysis. During all experiments listed in table 1, the magnetic flux density evolution for the 45 min waiting period that followed the magnetization process was measured at different distances above the surface of the superconductor. The measurements were then analysed using the flux creep model introduced by Zeldov [43–45], according to which the time evolution can be described with the following relation:

Published in : Supercond. Sci. Technol (2024), vol. 37, 16pp
DOI: 10.1088/1361-6668/ad68d1
Status : Postprint (Author's version)

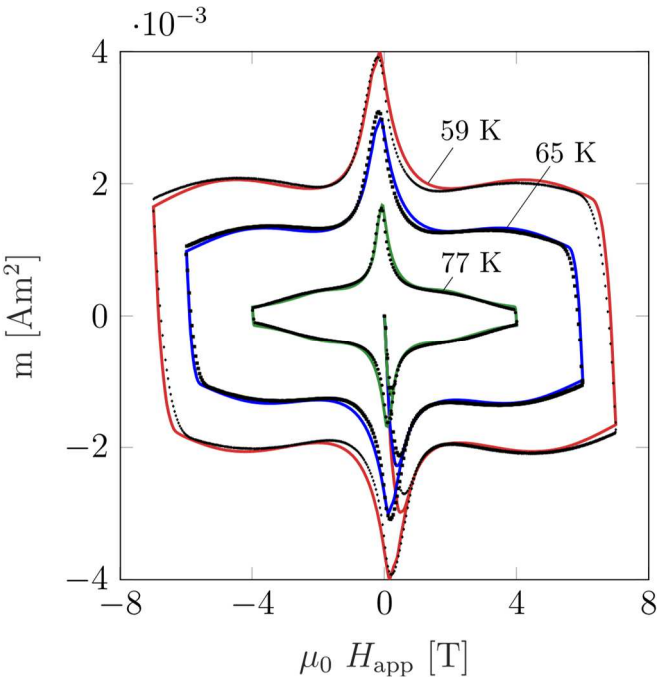

Figure 3. Comparison between the measured magnetic moment loop curves and those computed with the finite element model using a field-dependent critical current density as described by equation (1) with the parameters given in table 2. The markers represent the experimental data acquired at 77 K, 65 K and 59 K while the plain lines are the predictions of the finite element model.

$$\left(1+\frac{t}{t_0}\right)^{1-\frac{1}{n}}$$

$$B(t)= B_0, \qquad (2)$$

where the origin of time corresponds to the end of the field decreasing step of the magnetization process.

After adjusting equation (2) to the measurements, the values of the critical exponent, n were consistently found within the range of 37–42 for all explored temperatures. These critical exponent values align remarkably well with those derived for the cylindrical superconductors from which the cubic samples were extracted [27] and justify the value n = 40 used in the finite element model.

4.1.2. M(H) loop. This section focuses on the measurements carried out on the orthorhombic $YBa_2Cu_3O_{7-x}$ bulk superconductor. At each investigated temperature, the measurements were used to refine the parameters of the $J_c(B)$ law presented in equation (1). The values of the parameters obtained at each temperature after the fitting process are presented in table 2 and the magnetization loops computed with the finite element model using these specific values are compared to experimental data in figure 3. For information, the critical current density value at zero field as predicted by equation (1) is also presented in table 2.

As can be observed in figure 3, the measured magnetic moment loops of the orthorhombic sample exhibited a clearly visible fishtail effect, as is commonly observed for bulk superconductors in the literature [46–50]. In the rest of the work, it is assumed that the cubic superconducting samples exhibit an identical dependence of the critical current density on the applied magnetic field to the one derived in this section.

Published in : Supercond. Sci. Technol (2024), vol. 37, 16pp
DOI: 10.1088/1361-6668/ad68d1
Status : Postprint (Author's version)

Table 2. Values of the numerical parameters involved in the extended Kim's model (equation (1)) after adjustment to the magnetization curves measured at 77 K, 65 K and 59 K.

T (K)	$J_{c,0}$ (kA cm^{-2})	B_0 (mT)	a (–)	b_1 (–)	b_2 (–)	$J_c(0)$ (kA cm^{-2})
77	99	125	8	15	10	101
65	137	306	35	13	11	153
59	193	274	94	17	16	224

4.1.3. Trapped-field measurements. In this section, the magnetic flux density trapped by one of the cubic stationary sample (sample 1) was measured 2.7 mm above its surface and plotted as a function of the background field remaining at the end of the magnetization process. Figure 4 shows these measurements carried out at 77 K and 65 K compared to the finite element model predictions.

Figure 4(a) deals with results obtained at 77 K. At zero background DC field, the predicted value exceeds the measured one by 3 mT. This discrepancy is considered satisfactory considering that the critical current density was determined from measurements carried out on a different sample. When increasing the background magnetic field at the end of the magnetization process, the agreement between simulation and measurement remains satisfactory. Similar observations can be made at 65 K (figure 4(b)). The results plotted in figure 4 suggest that the diminution of the trapped field due to the nonzero background field can be successfully reproduced using the $J_c(B)$ dependence introduced in the finite element model at 77 K and at 65 K.

4.2. Single sample rotated in a background field

Before considering configurations involving multiple superconductors, we investigated the field trapped by a superconductor after a rotation of 180° in a background field. The goal of these sets of experiments is to investigate increased flux density gradient resulting from this rotation, as well as the possible demagnetization caused by the rotation process.

4.2.1. Fully penetrated sample rotated in a field. Figure 5 shows the magnetic flux density measured 4.2 mm above the surface of the rotating sample (sample 2) at the end of the experimental procedure presented in section 2.3 as a function of the background field. The measurements were compared to the predictions of the finite element model. The current distributions within the *x-z* cut plane including the centre of the superconductor, computed before and after the rotation, are presented in figures 5(b), (c), (e) and (f) for two particular background fields (100 mT and 300 mT).

We first consider measurements results at 77 K (red dots in figure 5(a)). Comparing the first two data points: one observes that a 180◦ rotation performed within a background magnetic field of 100 mT has minimal influence on the trapped magnetic field measured above the surface of the superconductor. This gives evidence that the superconducting material retains nearly its entire trapped-field ability provided that the background magnetic field during the rotation remains below the 100 mT threshold. Above this threshold, the magnitude of the trapped magnetic field exhibits a decreasing trend as the background DC magnetic field is increased. Remarkably, a similar behaviour is observed for the numerical simulations (blue squares in figure 5(a)): 180◦

Published in : Supercond. Sci. Technol (2024), vol. 37, 16pp
DOI: 10.1088/1361-6668/ad68d1
Status : Postprint (Author's version)

rotations within background magnetic fields smaller than 100 mT are even expected to increase slightly the final trapped magnetic field. This predicted increase may be understood considering the component of Bbg aligned with the c-axis of the sample. This component acts as a re-magnetizing field during the second half of the rotation process, reinforcing the superconducting current loops already present in the superconductor.

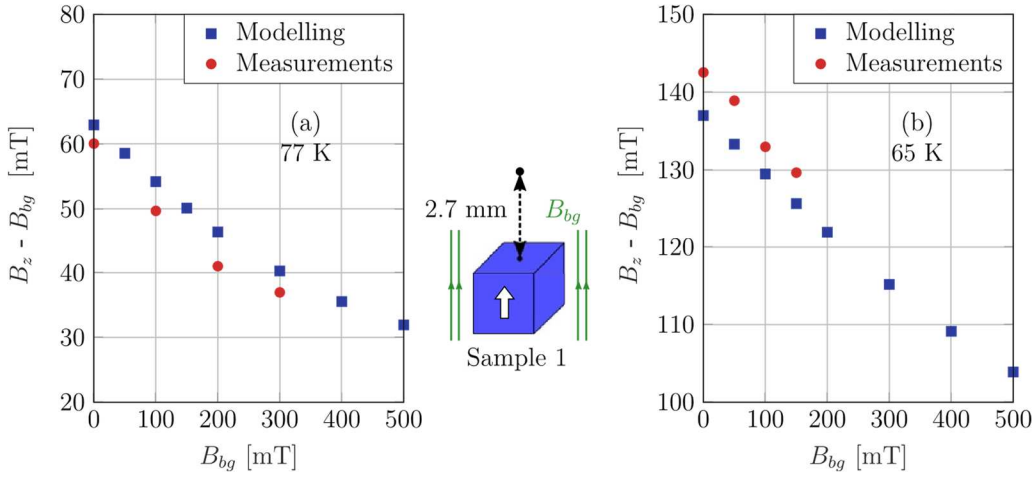

Figure 4. Comparison between the modelled and the experimental trapped field evaluated 2.7 mm above the surface of the stationary superconducting sample for different values of the background field. (a) 77 K; (b) 65 K.

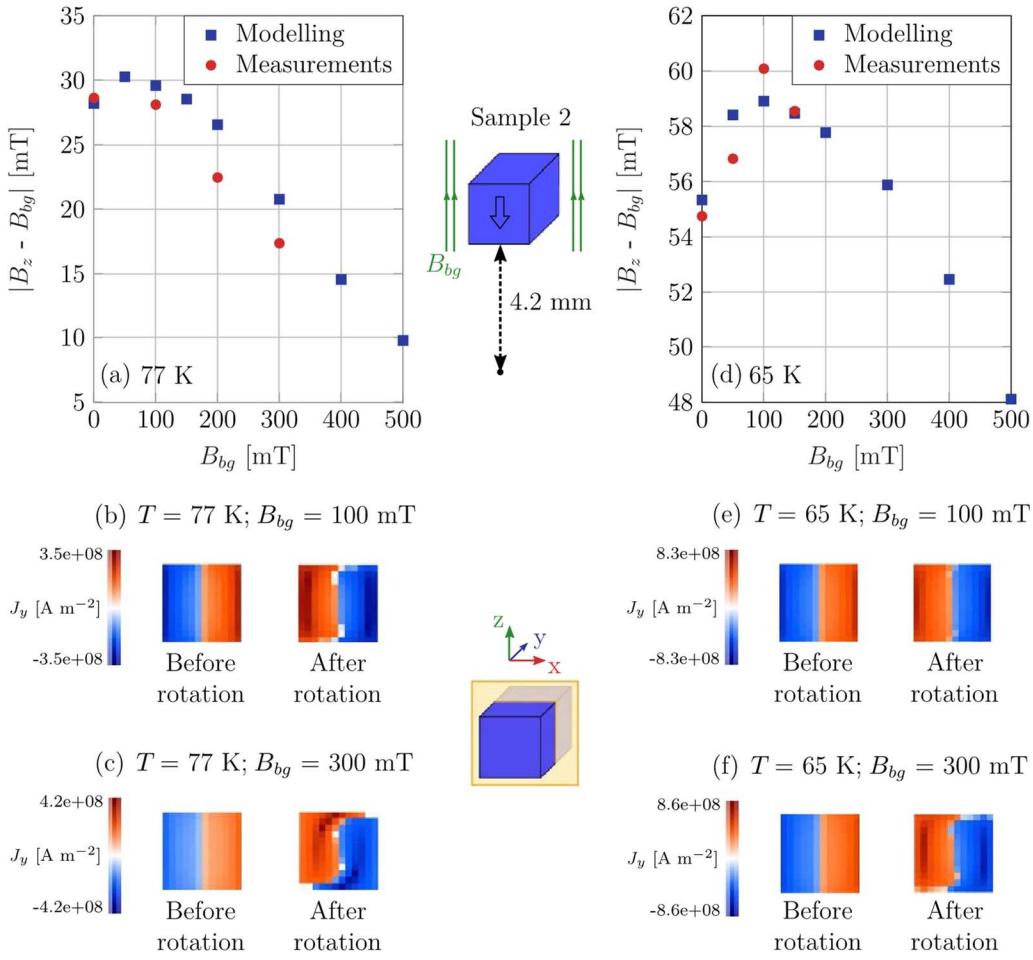

Published in : Supercond. Sci. Technol (2024), vol. 37, 16pp
DOI: 10.1088/1361-6668/ad68d1
Status : Postprint (Author's version)

Figure 5. (a) and (d) Comparison between the modelled and the experimental trapped field evaluated 4.2 mm above the surface of the rotated superconducting sample at the end of the procedure outlined in section 2.3 ($B_{max} \neq B_{bg}$) for various values of the background field at 77 K and 65 K respectively. (b), (c), (e) and (f) Current density distribution within the *x-z* cut plane encompassing the centre of the superconductor computed with the finite element model before and after the rotation for specific values of the temperature and background field.

It is of interest to investigate the current density distribution computed numerically before and after the rotation. Figure 5(b) shows the results for a 100 mT background field. Before the rotation, the *x-z* cut plane is divided into two halves where the supercurrents J_y display opposite signs, as can be expected for a cubic superconductor in the critical state. After the rotation, it can be noticed that the amplitude of the current density is altered, however, the qualitative distribution remains approximately identical. Considering the results at 300 mT (figure 5(c)) instead of 100 mT, the supercurrents J_y changes signs in two symmetric regions of the sample cross-section: (i) at the bottom left and (ii) at the top right. This re-organization of the current loops is consistent with the reduction of the measured trapped field. Similar current re-distributions have already been encountered in the literature in the context of rotating field experiments [51]. Such a similarity is not surprising since the rotation of the sample in a background field is equivalent to rotating the field around a stationary sample.

A similar approach is employed for analyzing the results obtained at 65 K. The experimental data are shown in figure 5(d). Starting from a zero background field, the trapped field measured after the 180° rotation is found to increase with increasing background field strength, reaches a maximum for B_{bg} = 100 mT and then starts decreasing. The same trend is found in the numerically computed values, which suggests that the finite element model captures correctly the overall behaviour measured at this temperature regime as well. Interestingly, it can be noticed that for all the non-zero background field strengths investigated experimentally at 65 K ([50—150] mT), the trapped field measured after the rotation exceeds the one measured in zero background field. Numerical

Published in : Supercond. Sci. Technol (2024), vol. 37, 16pp
DOI: 10.1088/1361-6668/ad68d1
Status : Postprint (Author's version)

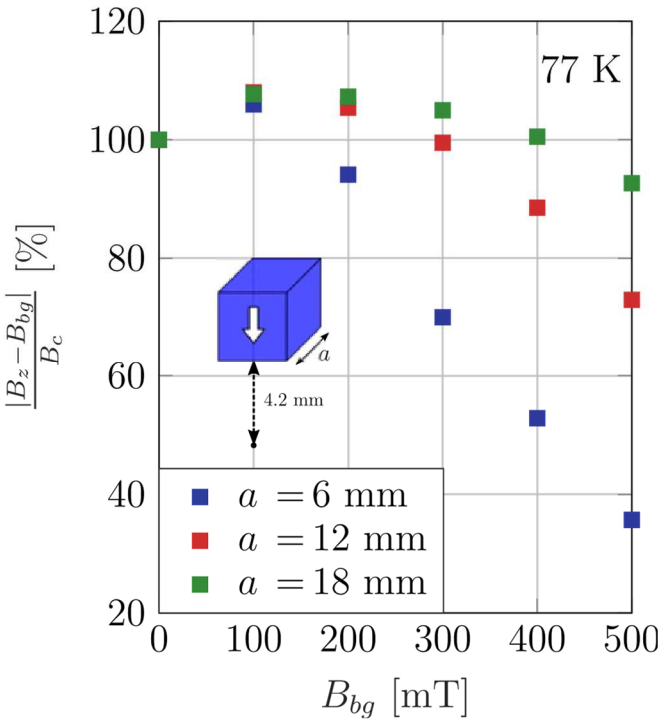

Figure 6. Numerical evaluation of the trapped field 4.2 mm above the surface of a superconducting cube of side length a at the end of the procedure outlined in section 2.3 (B_{max} ∀ B_{bg}) for various values of the background field. The results are normalized with respect to B_c which corresponds to the trapped field evaluated 4.2 mm above the surface of the sample in no background field.

simulations support this observation and predict that this holds true as long as $B_{bg} \leq 300$ mT. Comparing this threshold background field to the limit of 150 mT found at 77 K, decreasing the temperature is not only beneficial in increasing the field and field gradient achievable but also in extending the range of background field in which the superconductor can be rotated without demagnetization. Finally, figures 5(e) and (f) show that supercurrents J_y do not change sign in the top right and bottom left region of the cut plane for background field smaller than or equal to 300 mT.

Additional finite element simulations are conducted on superconducting cubes of various side lengths to explore, at 77 K, the impact of the size of the sample on the threshold background field. In these simulations, the field dependence of the critical current density is the same as above. Figure 6 shows the magnetic flux density computed 4.2 mm above the surface of the sample as a function of the background field in which the rotation is performed. Since the trapped field of the superconducting cube increases with its side length, the results are normalized relative to B_c which corresponds to the trapped field evaluated 4.2 mm above the surface of the sample in the absence of background field.

From figure 6, for a superconducting cube with dimensions of 6 mm, the complete preservation of trapped field ability during rotation (i.e. $(B_z\text{-}B_{bg})/B_c \geqslant 100\%$) is possible as long as the background magnetic field (B_{bg}) remains below 100 mT. For larger samples, it appears that this threshold field increases to 300 mT and 400 mT for cubes with side lengths of 12 mm and 18 mm, respectively. Consequently, it can be inferred that the use of larger samples extends the range of background magnetic fields within which the superconductor can undergo rotation without demagnetization.

Published in : Supercond. Sci. Technol (2024), vol. 37, 16pp
DOI: 10.1088/1361-6668/ad68d1
Status : Postprint (Author's version)

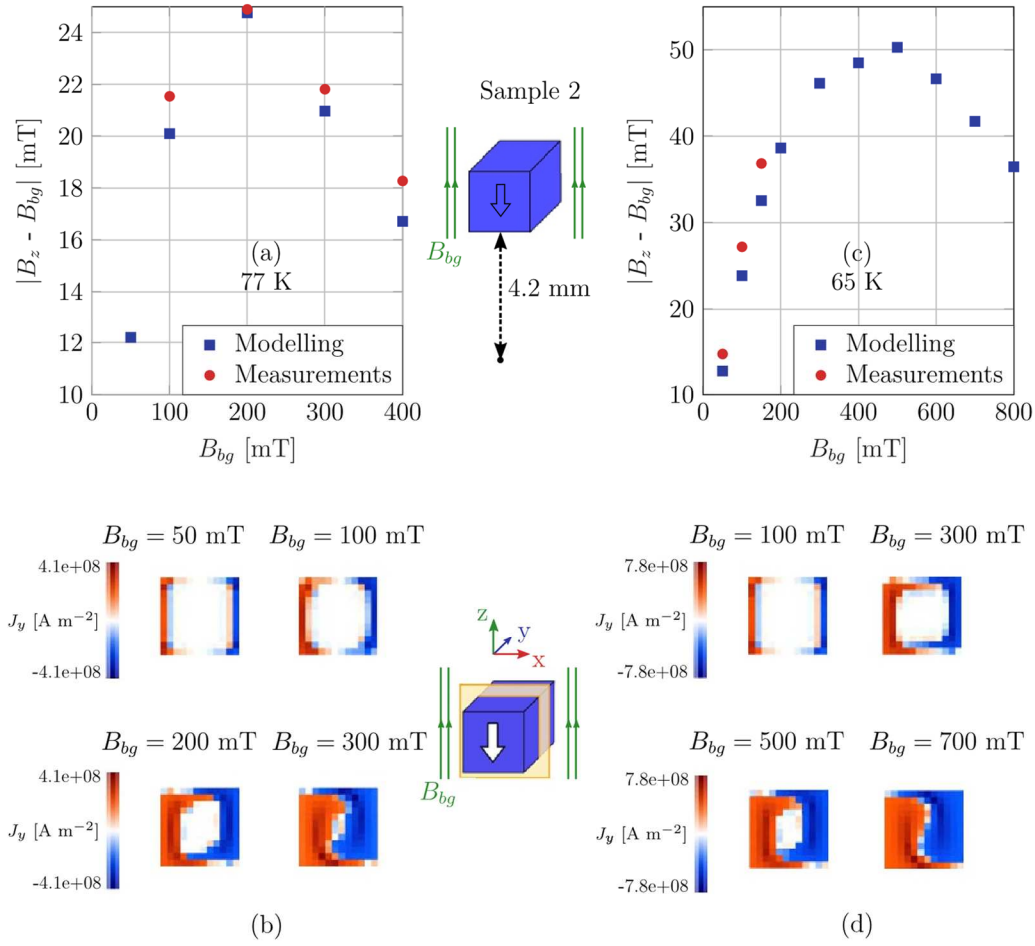

Figure 7. (a) and (c) Comparison between the modelled and the experimental trapped field evaluated 4.2 mm above the surface of the rotated superconducting sample after a field-cooling procedure followed by a 180° rotation in the same background DC field ($B_{max} = B_{bg}$) at 77 K and 65 K respectively. (b) and (d) Current density distribution within the *x-z* cut plane including the centre of the superconductor computed with the finite element model after the 180° rotation of the sample for specific values of the background field at 77 K and 65 K respectively.

4.2.2. Field-cooled sample rotated in a field. This section discusses an alternative magnetization procedure involving the FC of a superconducting sample within a constant DC magnetic field, followed by a rotation of 180° within the same DC field ($B_{max} = B_{bg}$). This magnetization process is particularly pertinent for scenarios where the applied magnetic field cannot be controlled or swept to magnetize the sample. This is e.g. the case when considering the use of an MRI scanner to generate the background field [14, 52–57]. The magnetic flux densities measured 4.2 mm above the surface of the rotating sample for different background field values are compared to the predictions of the finite element model in figure 7.

Figure 7(a) shows an excellent agreement between modelling and experiment: the finite element model reproduces the non-monotonic trend of the trapped field with increasing background field strength observed experimentally. Furthermore, it accurately anticipates that, within the range of background field strengths investigated experimentally, 200 mT emerges as the optimum level, yielding the highest trapped field

Published in : Supercond. Sci. Technol (2024), vol. 37, 16pp
DOI: 10.1088/1361-6668/ad68d1
Status : Postprint (Author's version)

magnitude. This agreement increases our confidence in the current density distribution computed and presented in figure 7(b). In this figure, the extent of supercurrent penetration within the superconducting sample deepens as the background magnetic field strength is increased. Interestingly, the analysis also reveals that after a 180° rotation in a background field of 200 mT, the sample is not yet fully penetrated with supercurrents despite this configuration yields the highest trapped magnetic field. Figure 7(c) shows that, at 65 K as well, the finite element model captures correctly the general measured trend of the trapped magnetic field as the background field strength is increased. The simulations indicate that the maximum trapped-field ability of the sample is achieved when it is subjected to a 500 mT background field during rotation. For mechanical reasons, the experimental investigations at this temperature exclusively explored background field strengths below this threshold value. This explains why the non-monotonic trend of the trapped field is not observed experimentally at 65 K.

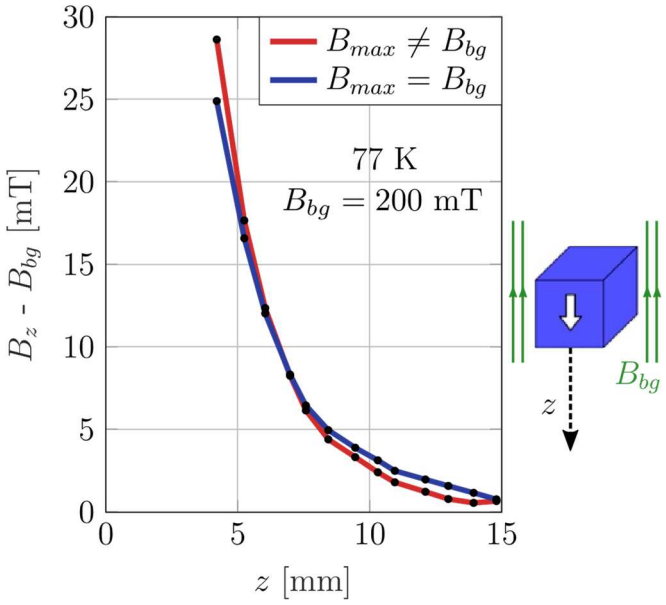

Figure 8. Comparison between the magnetic flux density profile measured at 77 K at the end of the procedure outlined in section 2.3 ($B_{max} \neq B_{bg}$) and after a field-cooling procedure followed by a 180° rotation in the same DC field ($B_{max} = B_{bg}$).

Considering that, at 77 K, the measured trapped field achieved with the alternative magnetization process reaches a maximum when B_{bg} = 200 mT, it is of interest to compare the magnetic flux density profile to that measured previously in the same background field when the sample was fully penetrated before the rotation. This comparison is presented in figure 8.

As can be observed in figure 8, the magnetic flux density profiles, and consequently the generated gradients, obtained with both magnetization methods are very similar. This confirms experimentally that FC and rotating a superconducting sample in an appropriate DC magnetic field is also a promising method for generating a magnetic flux density gradient in the presence of a background field.

4.3. Configurations using two samples

Published in : Supercond. Sci. Technol (2024), vol. 37, 16pp
DOI: 10.1088/1361-6668/ad68d1
Status : Postprint (Author's version)

4.3.1. Zero background field. In the previous section, the demagnetization of a superconductor rotated in a constant background field was investigated. In experiments involving two bulk superconductors, another potential source of current density alteration during rotational motion appears: the rather short distance between the magnetized superconductors during the rotation may result in a mutual demagnetization effect, similar to observations performed in the context of assembling superconducting Halbach arrays [37, 58]. This effect should be overcome to achieve gradients when combining two superconductors in a background DC field. In the following, configurations using two superconductors were first investigated in the absence of any background field. The purpose of this series of experiments was to determine whether a demagnetization effect arises due to the interaction between the two cubic samples positioned at a separating distance of 16.6 mm.

The simultaneous magnetization of the superconductors followed by the 180° rotation of the top sample is modelled using the finite element model both at 77 K and 65 K. The current density distribution in the *x-z* cut plane including the centres of both superconductors computed before and after the rotation is shown in figure 9.

Figure9(a)shows that within each sample, the current density distribution remains unchanged after the rotational process, when compared to the distribution computed before any motion. This observation implies that, for such a separating distance, there is no discernible magnetic interaction between the samples. The same conclusion can be drawn at 65 K

(figure 9(b)).

The configuration with two samples and no background field is then investigated experimentally. In figures 10(a) and (b), the measured magnetic flux density profile is compared to that measured when only one sample, either sample 1 or sample 2, is placed in the experimental setup. Based on the measured profile, a cubic smoothing spline method is employed and the derivative of this smoothed curve is computed to approximate the magnetic flux density gradient in each experiment, the results are shown in figures 10(c) and (d).

At 77 K (figure 10(a)), and more particularly in the region close to the stationary sample 1 ($z \leqslant 5$ mm), the profile measured for two samples is close to the measurements obtained when this sample 1 is alone. Similarly, in the region close to the rotating sample 2 ($z \geqslant 10$ mm), the profile in the configuration involving both samples is almost superimposed with the one measured in the presence of sample 2 only. These observations confirm experimentally that the distance between the superconducting samples is large enough to avoid any demagnetization due to the interaction between them during the rotation. In the intermediate region ($5\text{ mm} \leqslant z \leqslant 10$ mm), each sample provides a nonnegligible contribution to the total magnetic flux density. The profile measured in the configuration with two superconductors can be viewed as the sum of each individual contribution. The magnetic flux density gradient computed is plotted in figure 10(c). With the two-sample configuration, the gradient exceeds 3.8 T m^{-1} across the whole intermediate region, which is not the case for single-sample configurations. The samples are therefore placed close enough to shape the magnetic flux density profile and generate, in between them, a higher field gradient than when they are employed alone.

As can be observed in figures 10(b) and (d), the behaviour measured at 65 K is qualitatively the same as at 77 K. The major difference is that, at 65 K, the magnetic flux density gradient exceeds 8.4 T m^{-1} across the whole intermediate region.

Published in : Supercond. Sci. Technol (2024), vol. 37, 16pp
DOI: 10.1088/1361-6668/ad68d1
Status : Postprint (Author's version)

The question that naturally arises is whether these values of magnetic flux density gradients are affected by a background field. This topic is addressed in the next section.

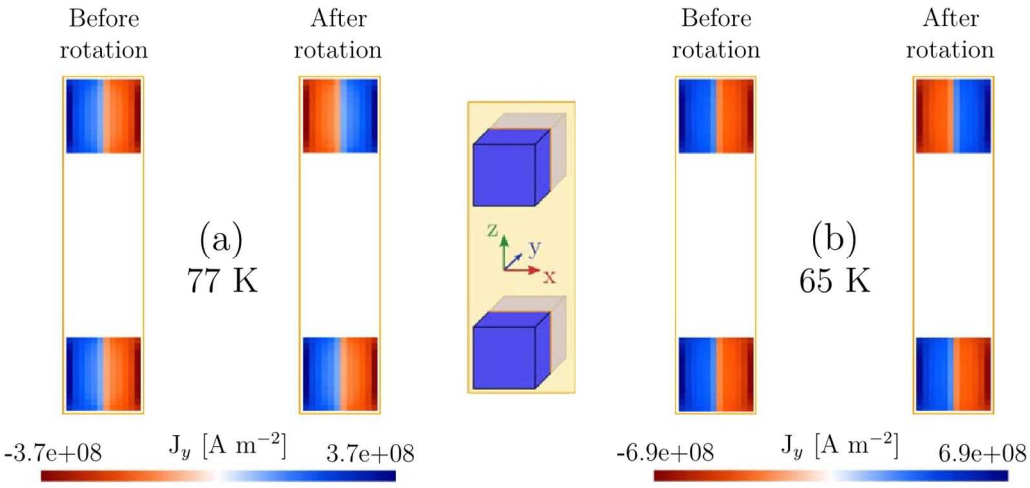

Figure 9. Current density distribution in the *x-z* cut plane encompassing the centres of both superconductors computed with the finite element model before and after the rotation and in the absence of any background field. (a) 77 K; (b) 65 K.

Published in : Supercond. Sci. Technol (2024), vol. 37, 16pp
DOI: 10.1088/1361-6668/ad68d1
Status : Postprint (Author's version)

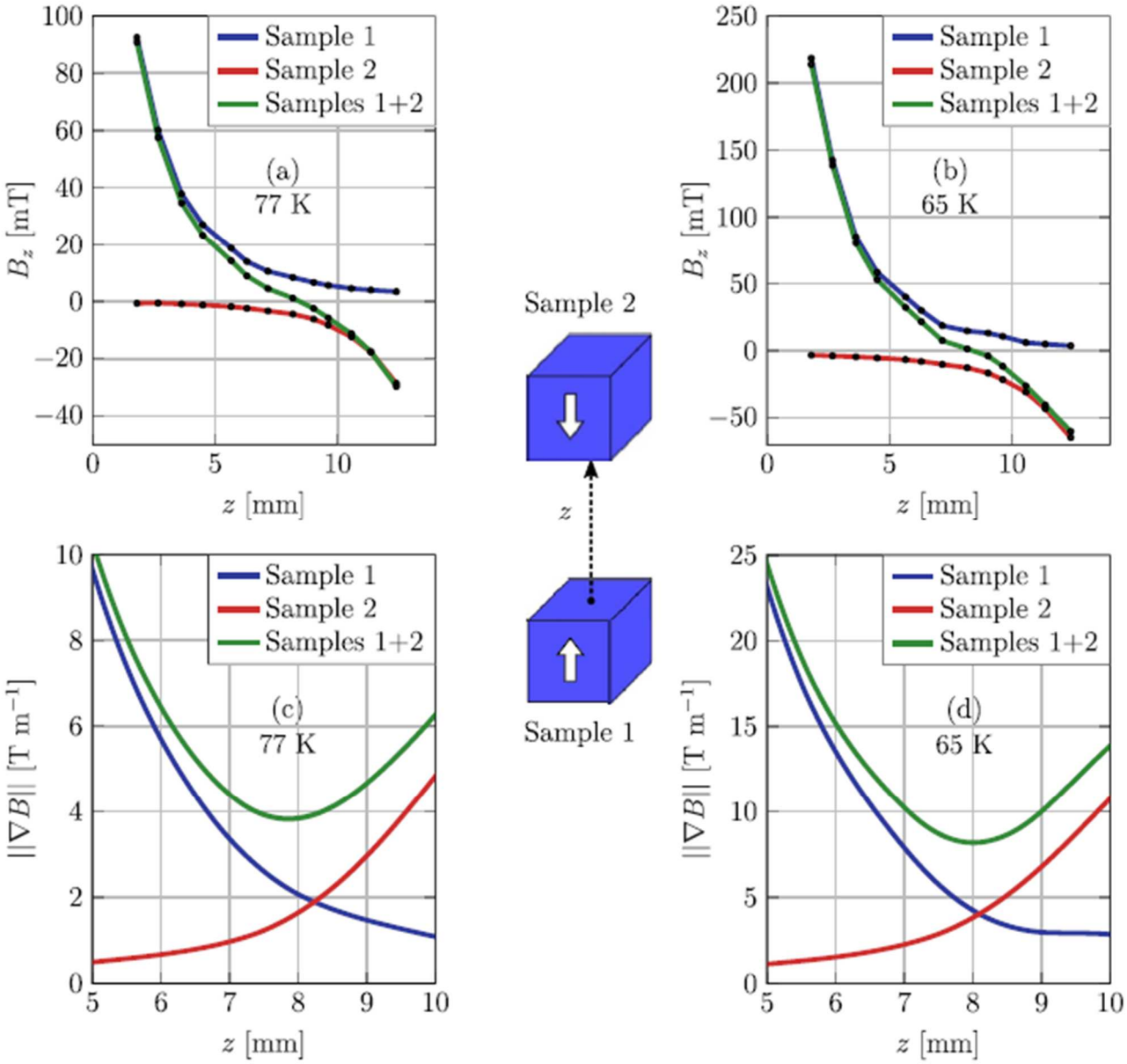

Figure 10. (a) and (b) Magnetic flux density profile measured at the end of the procedure outlined in section 2.3 ($B_{max} \neq$ B_{bg}) for single and dual sample configurations with no background field at 77 K and 65 K respectively. (c) and (d) Gradient of the magnetic flux density profile for single and dual sample configurations with no background field at 77 K and 65 K respectively.

Published in : Supercond. Sci. Technol (2024), vol. 37, 16pp
DOI: 10.1088/1361-6668/ad68d1
Status : Postprint (Author's version)

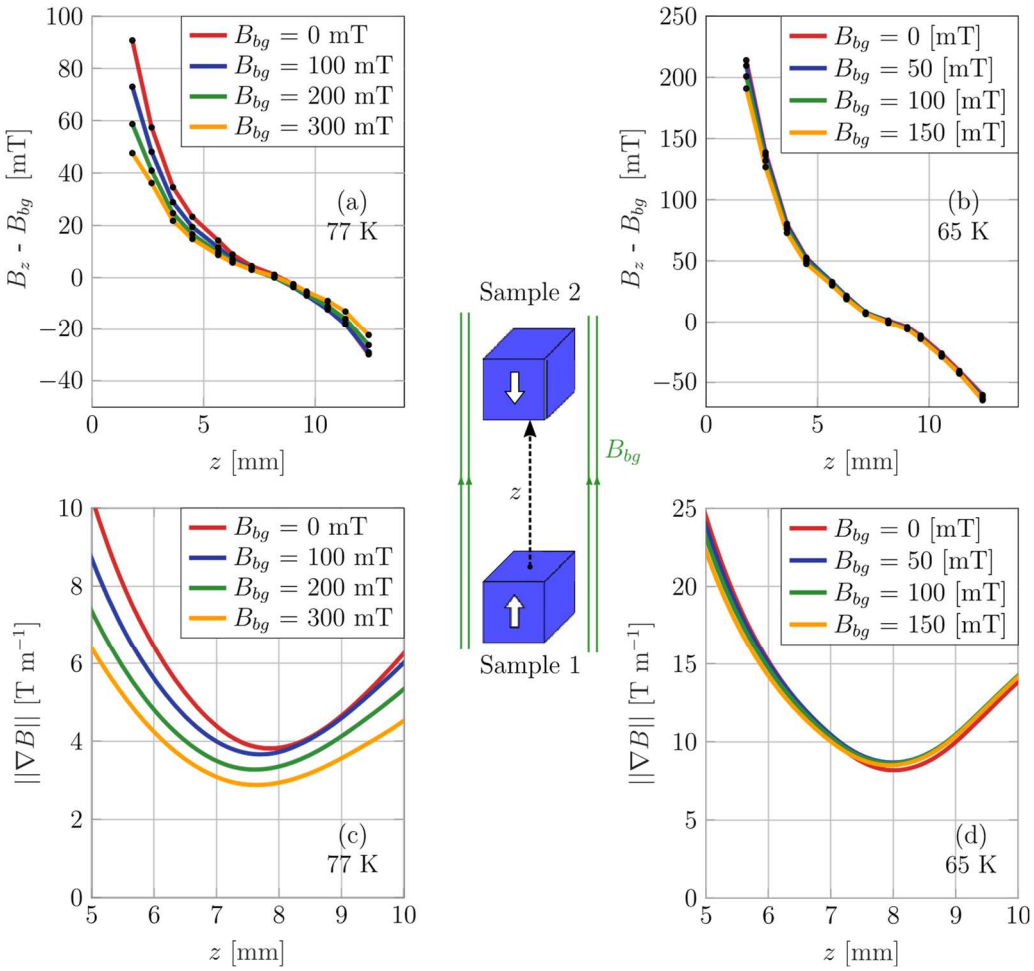

Figure 11. (a) and (b) Magnetic flux density profile measured at the end of the procedure outlined in section 2.3 ($B_{max} = B_{bg}$) for dual sample configuration for various values of the background field at 77 K and 65 K respectively. (c) and (d) Gradient of the magnetic flux density profile for dual sample configuration for various values of the background field at 77 K and 65 K respectively.

Published in : Supercond. Sci. Technol (2024), vol. 37, 16pp
DOI: 10.1088/1361-6668/ad68d1
Status : Postprint (Author's version)

4.3.2. Non-zero background field. The configuration investigated in this section combines the challenges discussed previously: the preservation of a non-zero background magnetic field and the 180° rotation of a superconductor while being in proximity to another magnetized sample. The magnetic flux density profiles and gradients are shown in figure 11.

At 77 K, in the region close to the stationary sample ($z \leqslant 5$ mm in figure 11(a)), the total magnetic flux density is found to decrease with increasing background DC field, which can be attributed to the $J_c(B)$ dependence. In the region close to the rotating sample ($z \geqslant 10$ mm), a decrease in the trapped field measured is only apparent when $B_{bg} \geqslant 200$ mT, which is a consequence of the current re-organization induced by the rotation of sample 2 in the background field. The magnetic flux density gradient generated in the intermediate region (figure 11(c)) decreases with increasing background DC field. In a background of 300 mT at 77 K, the measured gradient throughout the intermediate region exceeds 2.9 T m^{-1}. This is not achievable when using only one of the samples even in a zero background DC field (see figure 10(c)). Figures 11(b) and (d) respectively show that, at 65 K, the different magnetic flux density profiles measured can hardly be distinguished from one another and that the magnetic flux density gradient exceeds 8.4 T m^{-1} across the entire intermediate region whatever the background field strength in the range 0 mT to 150 mT.

Two duplicate experiments are conducted at 59 K to illustrate the potential of the configuration at even lower temperatures. The flux density profiles and gradients measured are presented in figure 12.

In figure 12(b), it appears that, at 59 K, the minimal magnetic flux density gradient generated by the assembly in the intermediate region surpasses 10 T m^{-1} with no background field. The gradient exceeds 10.8 T m^{-1} when $B_{bg} = 50$ mT.

To put such performances into perspective, instead of superconducting samples, two Nd–Fe–B cubic permanent magnets with 6 mm sides were placed in the experimental system. The minimal field gradient generated with such samples at room temperature in zero background field was measured to be 11.5 T m^{-1} in the intermediate region. This value is used as a benchmark to which the gradients measured in zero background field with the configuration with two superconductors at various temperatures are compared in figure 13(a). It is important to note that the remanent magnetization of the configuration for various values of the background field at 59 K.

Published in : Supercond. Sci. Technol (2024), vol. 37, 16pp
DOI: 10.1088/1361-6668/ad68d1
Status : Postprint (Author's version)

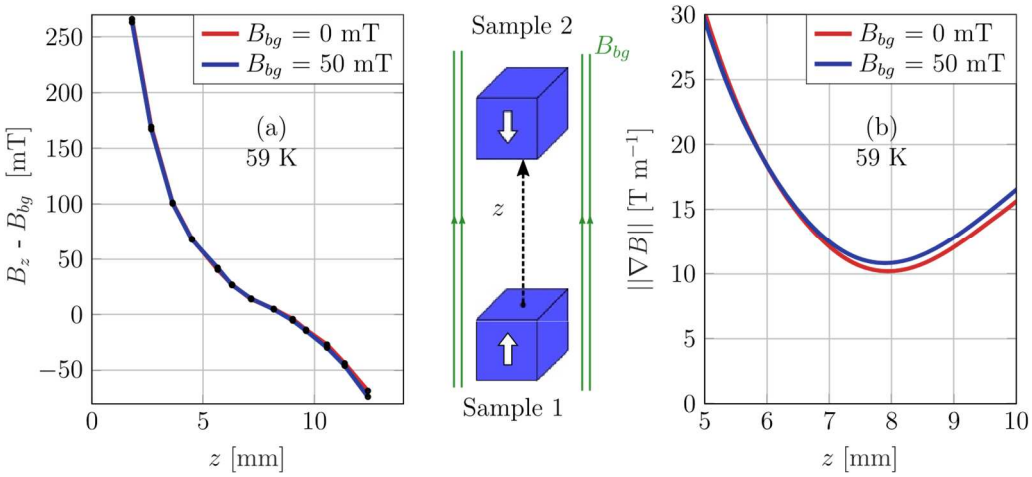

Figure 12. (a) Magnetic flux density profile measured at the end of the procedure outlined in section 2.3 ($B_{max} = B_{bg}$) for dual sample configuration for various values of the background field at 59 K. (b) Gradient of the magnetic flux density profile for dual sample

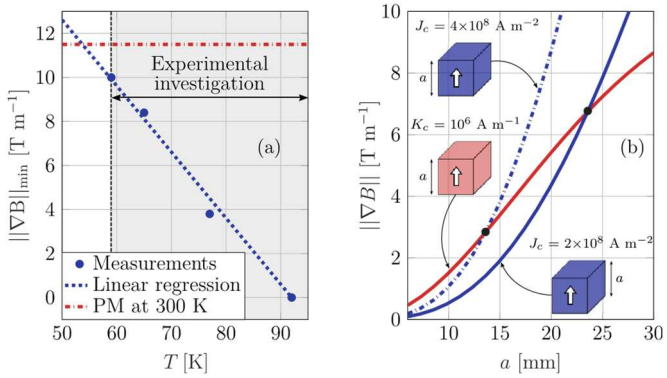

Figure 13. (a) Minimal magnetic flux density gradient measured in the intermediate region with the configuration with two superconductors at various temperatures in zero background field. (b) Magnetic flux density gradient computed at a distance of 20 mm from the surface of a cubic permanent magnet (in red) or trapped-field magnet (in blue).

Nd–Fe–B permanent magnet exhibits a non-monotonic evolution with temperature. Starting from its value at 300 K, the remanent magnetization initially increases as the temperature decreases, then undergoes a spin-reorientation transition, and subsequently decreases. Measurements indicate that the remanence in the range 59 K–77 K is close to the one at 300 K [59–61]. In the temperature range investigated experimentally, permanent magnets outperform bulk superconducting $YBa_2Cu_3O_{7-x}$ samples of the same size. Nevertheless, contrary to permanent magnets, the gradient generated with superconductors is measured to increase almost linearly with decreasing temperatures. Operating the superconducting assembly at ~50 K and below is therefore expected to surpass the performances of permanent magnets. Furthermore, a semi-analytical model based on Biot-Savart's law is used to evaluate the gradient produced 20 mm above the surface of a cubic sample (either a permanent magnet or a trapped-field magnet) of various side lengths. The model assumes that the field generated by a permanent magnet can be modelled by a surface current denoted K_c flowing at the

Published in : Supercond. Sci. Technol (2024), vol. 37, 16pp
DOI: 10.1088/1361-6668/ad68d1
Status : Postprint (Author's version)

periphery of the magnet. The results are presented in figure 13(b) and confirm that larger superconductors are expected to outperform permanent magnets. The size corresponding to the cross-over is found to be around ~24 mm when a field-independent J_c of 2×10^8 A m^{-2} is assumed, i.e. approximately the experimental J_c at 77 K of the $YBa_2Cu_3O_{7-x}$ samples used. Assuming a linear $J_c(T)$ dependence, one can expect a J_c of approximately 4×10^8 Am^{-2} at62K,which reduces the coss-oversize down to ~14 mm.

5. CONCLUSIONS

In this work, we show that $YBa_2Cu_3O_{7-x}$ bulk superconductors can be combined spatially without significant demagnetization. This demonstrates that these arrays of bulk superconductors open the prospect of producing larger field gradients than those that can be attained with an isolated bulk. This investigation was conducted in the presence of a uniform DC magnetic field at the end of the magnetization process for 3 temperatures: 77 K, 65 K and 59 K.

Although the non-zero applied field yields a reduction in the fields and field gradients generated by an individual and stationary sample, this phenomenon was measured to be significantly mitigated at 65 K and at 59 K compared to 77 K. Using a finite element model based on the mixed *h-*φ*-a* formulation, the parameters of a field-dependent relationship for the critical current density were adjusted to successfully reproduce magnetization loop measurements conducted at the three investigated temperatures. The comparison of the finite element model with the measurements highlighted that the decreased trapped field in the presence of a background field can be reproduced by considering the field dependence of the critical current density.

Next, the effect of a 180° rotation within a uniform magnetic field on the trapped field of an individual superconductor was investigated. Experimental and numerical results showed that, at 77 K, the full trapped-field ability of the superconducting sample is preserved, provided that the rotation occurs within a background magnetic field of 150 mT or less. This limit on the background field was found to increase to 300 mT when the temperature is decreased to 65 K. Further numerical simulations showed that enlarging the geometrical dimensions of the sample also increases this limit. It was also shown experimentally that FC and rotating a superconducting sample in an appropriate DC magnetic field generates a magnetic flux density gradient similar to that obtained when a complete magnetization of the sample is carried out before the rotation.

Then, the magnetic flux density gradient generated by a pair of superconductors with anti-parallel magnetizations was measured at various temperatures. In zero background field, the sample-to-sample distance (~16 mm) was shown to be sufficient to avoid any mutual demagnetization effect and the magnetic flux density gradient generated between the superconductors was measured to exceed 3.8 T m^{-1} and 8.4 T m^{-1} at 77 K and 65 K respectively. When considering a non-zero background field at 77 K, despite the alteration of the current distribution anticipated during the rotation, a gradient higher than 2.9 T m^{-1} was measured across the whole targeted region in the presence of a 300 mT background field. Enhanced performance was achieved at lower temperatures where magnetic

Published in : Supercond. Sci. Technol (2024), vol. 37, 16pp
DOI: 10.1088/1361-6668/ad68d1
Status : Postprint (Author's version)

flux density gradient exceeding 8.4 T m^{-1} (150 mT background field, 65 K) and exceeding 10.8 T m^{-1} (50 mT background field, 59 K) were demonstrated. These gradient values were shown to be comparable to those achieved with ferromagnetic permanent magnets of similar size. Further decreasing the operating temperature or increasing the size of the superconductors would increase the gradient generated. Under such circumstances, it is anticipated that the superconducting assembly have the full potential to surpass the capabilities afforded by permanent magnets.

DATA AVAILABILITY STATEMENT

All data that support the findings of this study are included within the article (and any supplementary files).

ACKNOWLEDGMENTS

This work was supported by the Fonds de la Recherche Scientifique − FNRS under Grant CDR No J.0218.20 (35325237). Michel Houbart is recipient of a FRS-FNRS Research Fellow Grant.

APPENDIX. DESIGN AND CALIBRATION OF THE MULTI-HALL PROBE

In the present work, the distribution of magnetic flux density is measured using several stationary Hall sensors. The home-made experimental system including the stationary Hall sensors is called the 'multi-Hall probe'. This multi-Hall probe consists of a stack of 7 PCB of 0.4 mm in height as shown in figure A1. In this configuration, each PCB in the stack, except for the base PCB, is equipped with two *Lakeshore* HGT-2101 Hall sensors, one is soldered on the top surface, the other on the bottom surface. Each stage is soldered to its neighbour which provides electrical contact from one stage to the next one and facilitates the feeding of all the sensors placed electrically in series, see figure A1(a). The multi-Hall probe is designed to be tightened directly on the stationary sample holder. When the probe is installed, the centres of the Hall sensors are aligned in the *z*-direction.

The calibration of the sensitivity and offset of the Hall sensors of the multi-Hall probe is performed at five specific temperatures within the PPMS: 60 K, 65 K, 70 K, 75 K and 80 K. For experiments conducted at other temperatures, a linear interpolation between the two closest measured values is performed to determine the calibration constants. At each temperature, the individual offset is evaluated by averaging the output signal of each Hall probe over a period of 300 s when no field is applied. When possible, the offset of each sensor is reassessed at the start of each experimental run; otherwise, the previously determined offset is used. Regarding calibration of the sensitivity, the applied field is increased from 0 to 2 T with steps of 50 mT while monitoring the output signal of each sensor. Subsequently, a linear regression is applied to derive the sensitivity values. In practice, the sensitivity is found to exhibit minimal variations with temperature within the explored temperature range. The sensitivity of all sensors is found to fall in the range [0.19–0.23] mV/mT. Although the sensors are operated outside the temperature range recommended by the manufacturer (i.e. between 218 K and 398 K), it is remarkable to observe that the experimentally determined sensitivities remain well within

Published in : Supercond. Sci. Technol (2024), vol. 37, 16pp
DOI: 10.1088/1361-6668/ad68d1
Status : Postprint (Author's version)

the range specified in the datasheet. It should be pointed out that for measurements performed at 59 K, the calibration constants determined at 60 K are used. This is expected to result in a minimal error considering that the variations of the calibration constants were measured to be smaller than 0.5% between 65 K and 60 K.

The same calibration procedure is also conducted at ambient temperature, for which the sensitivity of the Hall probes is measured to lie in the range [0.15–0.18] mV/mT.

After establishing the calibration constants for each individual Hall sensor, a preliminary experiment is conducted outside the PPMS in order to determine, at ambient temperature, the relative distance between the active surfaces of the Hall sensors. A schematic illustration of this experiment is shown in figure A2(a).

A cubic Nd–Fe–B permanent magnet of 10 mm side and main magnetization direction along the *x*-direction is moved along a line parallel to the *z*-direction. The motion is achieved using a 3D micro-positioning system from Thorlabs® (MTS S50-Z8). The multi-Hall probe is positioned as close as possible to the path of the permanent magnet and is oriented such that the Hall sensors measure the *z*-component of the magnetic flux density generated by the permanent magnet. In such a configuration, the output signal of a specific Hall sensor vanishes when the geometric centre of the permanent magnet is aligned with the active surface of that particular sensor. Therefore, by monitoring the evolution of the output signal of each Hall probe as a function of the permanent magnet position and comparing the positions at which each individual signal is zero, the relative distance between the active surfaces can be derived. As an illustration, the evolution of the flux density measured by 4 Hall sensors distributed in the multi-Hall probe as a function of the permanent magnet position is shown in figure A2(b). The permanent magnet position at which the signal of the highest Hall sensor in the stack vanishes is used as a reference position.

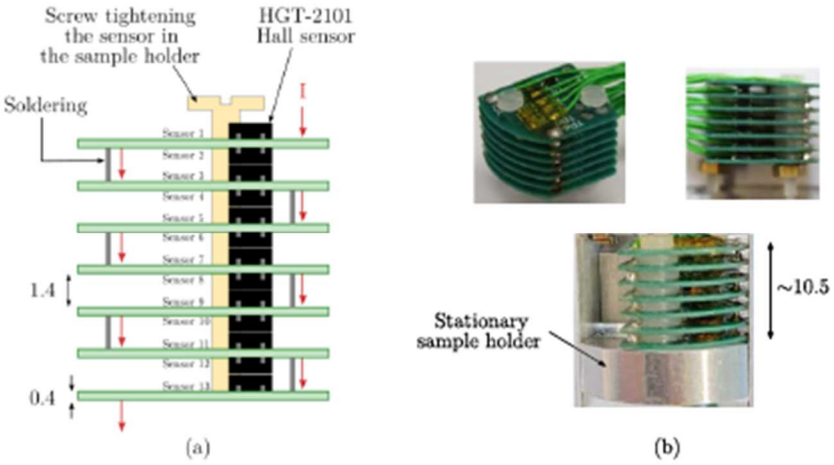

Figure A1. Bespoke multi-Hall probe used for the determination of the magnetic flux density gradient (a) Conceptual view; (b) Pictures of the actual sensor. All dimensions are in mm.

Published in : Supercond. Sci. Technol (2024), vol. 37, 16pp
DOI: 10.1088/1361-6668/ad68d1
Status : Postprint (Author's version)

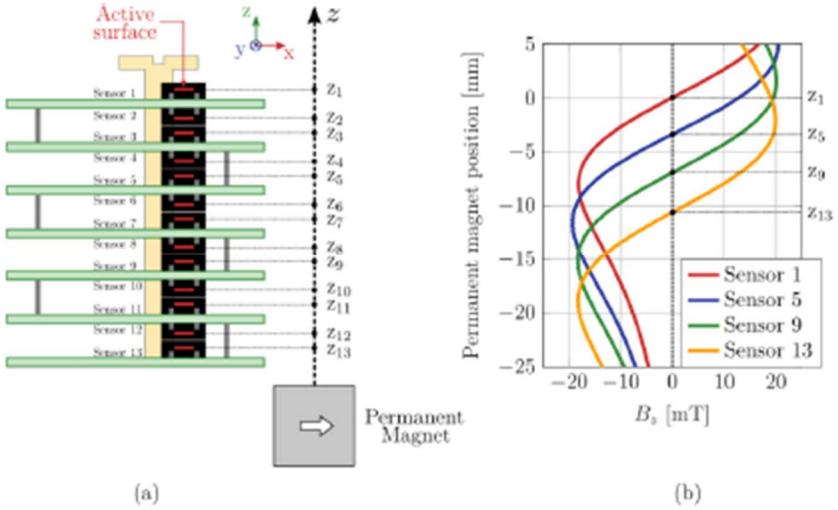

Figure A2. (a) Schematic illustration of the experiment to calibrate the relative distance between the active surfaces of the Hall probes within the gradient measuring sensor. (b) Evolution of the magnetic flux density measured by 4 Hall probes distributed in the multi-Hall probe as a function of the position of the permanent magnet moved along the *z*-direction.

The positions of all the other Hall probes relative to the reference are summarized in table A1.

Given possible mechanical deformations when operating the gradient measuring sensor at cryogenic temperatures, a second experimental run with the setup immersed in a liquid nitrogen bath is carried out. In an effort to minimize the thermal shock experienced by the sensors, the experimental setup is enclosed within a sealed chamber as shown in figure A3 before immersing it in liquid nitrogen. In this preliminary measurement, only19 electrical leads could be routed

Table A1. Relative distance between the active surfaces of the Hall sensors within the multi-Hall probe measured at 300 K and at 77 K. Th position of the uppermost probe in the stack (sensor 1) is used as a reference.

		$\lvert z_1\rvert$ (mm)	$\lvert z_2\rvert$ (mm)	$\lvert z_3\rvert$ (mm)	$\lvert z_4\rvert$ (mm)	$\lvert z_5\rvert$ (mm)	$\lvert z_6\rvert$ (mm)			$\lvert z_7\rvert$ (mm)	$\lvert z_8\rvert$ (mm)	$\lvert z_9\rvert$ (mm)	$\lvert z_{10}\rvert$ (mm)	$\lvert z_{11}\rvert$ (mm)	$\lvert z_{12}\rvert$ (mm)	$\lvert z_{13}\rvert$ (mm)
300 K	0	1	1.8				2.8	3.4	4.3	5.3	6.1	6.9	7.9	8.8	9.7	10.6
77 K	0	1.1	1.9				2.8	3.3	4.2	5.2	/	/	/	/	/	/

Published in : Supercond. Sci. Technol (2024), vol. 37, 16pp
DOI: 10.1088/1361-6668/ad68d1
Status : Postprint (Author's version)

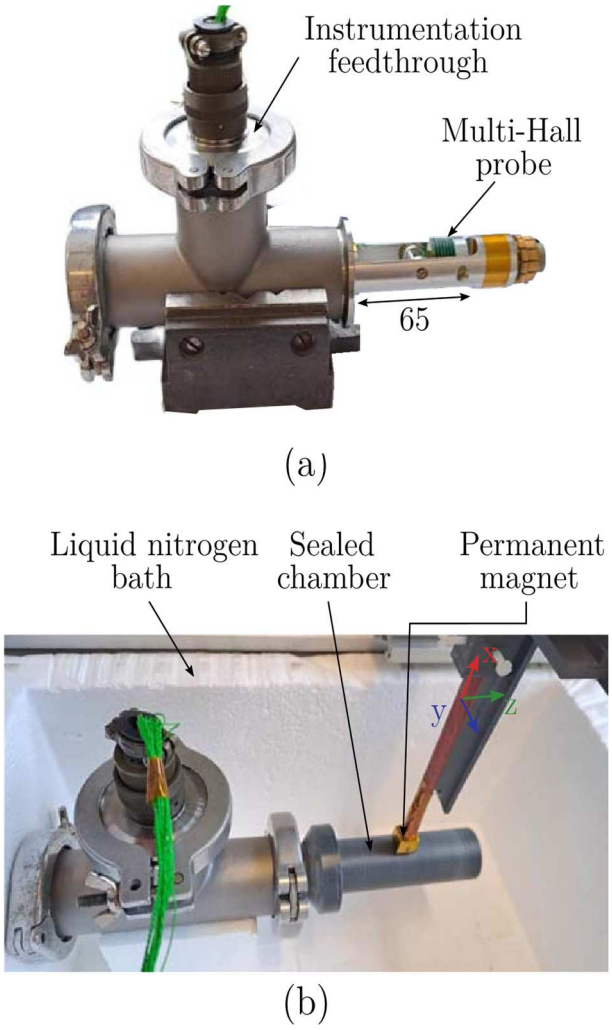

Figure A3. Photographs of the experimental setup used to calibrate the relative distance between the active surfaces of the Hall sensors within the multi-Hall probe at 77 K.

inside the enclosure. Among them, two are allocated for current leads. Additionally, another two pins are reserved for a Pt100 temperature sensor, which is integrated into the system to monitor the temperature within the enclosure and make sure that the experiment is carried out once the thermal equilibrium is reached. The signals given by only 7 Hall sensors can thus be acquired during the manipulation. The positions of all the acquired Hall sensors relative to the uppermost sensor in the stack are summarized in table A1. Two photographs of the experimental configuration are shown in figure A3.

Comparing the distance evaluated at ambient and cryogenic temperature, it can be noticed that the mechanical deformations due to the cryogenic environment do not induce significant modifications of the relative distance between the active surfaces of the Hall probes, at least for those monitored during the experiment performed at 77 K. In the following, it is assumed that the same hold s true for the Hall

Published in : Supercond. Sci. Technol (2024), vol. 37, 16pp
DOI: 10.1088/1361-6668/ad68d1
Status : Postprint (Author's version)

sensors that could not be measured during the experiment conducted in the liquid nitrogen bath. The distances determined at ambient temperature are used for these probes.

ORCID IDS

M Houbart https://orcid.org/0000-0003-4166-9029
J-F Fagnard https://orcid.org/0000-0002-8898-0298
P Harmeling https://orcid.org/0000-0003-4775-8495
J Dular https://orcid.org/0000-0003-0503-7526
A R Dennis https://orcid.org/0000-0003-4962-7149
D K Namburi https://orcid.org/0000-0003-3219-2708
J H Durrell https://orcid.org/0000-0003-0712-3102
C Geuzaine https://orcid.org/0000-0001-9970-358X
B Vanderheyden https://orcid.org/0000-0003-1247-3369
P Vanderbemden https://orcid.org/0000-0002-1436-7116

REFERENCES

[1] Barnsley L C, Carugo D, Owen J and Stride E 2015 *Phys. Med. Biol.* **60** 8303–27

[2] Barnsley L C, Carugo D and Stride E 2016 *J. Phys. D: Appl. Phys.* **49** 225501

[3] Kee H, Lee H and Park S 2020 *J. Magn. Magn. Mater.* **514** 167180

[4] Omelyanchik A, Lamura G, Peddis D and Canepa F 2021 *J. Magn. Magn. Mater.* **522** 167491

[5] Latulippe M and Martel S 2014 *Proc. IEEE 5th RAS/EMBS Int. Conf. Biomed. Robot. Biomechatronics* pp 320–5

[6] Latulippe M and Martel S 2015 *IEEE Trans. Robot* **31** 1353–63

[7] Latulippe M, Felfoul O, Dupont P E and Martel S 2016 *Appl. Phys. Lett.* **108** 062403

[8] Latulippe M and Martel S 2018 *IEEE Trans. Magn.* **54** 5600112

[9] Fohr F and Volbers N 2018 *AIP Adv.* **8** 047701

[10] Nariki S, Teshima H and Morita M 2016 *Supercond. Sci. Technol.* **29** 034002

[11] Tomita M and Murakami M 2003 *Lett. Nat.* **421** 517–20

[12] Durrell J H *et al* 2014 *Supercond. Sci. Technol.* **27** 082001

[13] Patel A, Baskys A, Mitchell-Williams T, McCaul A, Coniglio W, Hänisch J, Lao M and Glowacki B A 2018 *Supercond. Sci. Technol.* **31** 09LT01

[14] Arsenault A and Sirois F 2023 *IEEE Trans. Appl. Supercond.* **33** 4401409

[15] Funaki K and Yamafuji K 1982 *Jpn. J. Appl. Phys.* **21** 299–304

[16] Campbell A M, Baghdadi M, Patel A, Zhou D and Huang K Y, Shi Y-H and Coombs T A 2017 *Supercond. Sci. Technol.* **30** 034005

Published in : Supercond. Sci. Technol (2024), vol. 37, 16pp
DOI: 10.1088/1361-6668/ad68d1
Status : Postprint (Author's version)

[17] Hong Z, Vanderbemden P, Pei R and Jiang Y, Campbell A M and Coombs T A 2008 *IEEE Trans. Appl. Supercond.* **18** 1561–4

[18] Vanderbemden P, Hong Z, Coombs T A, Denis S, Ausloos M, Schwartz J, Rutel I B, Hari Babu N, Cardwell D A and Campbell A M 2007 *Phys. Rev.* B **75** 174515

[19] Fisher L M, Kalinov A V, Savel'ev S E, Voloshin I F, Yampol'skii V A, Leblanc M A R and Hirscher S 1997 *Physica* C **278** 169–79

[20] Srpcic J, Perez F, Huang K Y, Shi Y-H, Ainslie M D, Dennis A R, Filipenko M, Boll M, Cardwell D A and Durell J H 2019 *Supercond. Sci. Technol.* **32** 035010

[21] Luzuriaga J, Badía-Majós A, Nieva G, López C, Serquis A and Serrano G 2009 *Supercond. Sci. Technol.* **22** 015021

[22] Kapolka M, Srpcic J, Zhou D, Ainslie M D, Pardo E and Dennis A R 2018 *IEEE Trans. Appl. Supercond.* **28** 6801405

[23] Cardwell D A 1998 *Mater. Sci. Eng.* B **53** 1–10

[24] Shi Y-H, Namburi D K, Zhao W, Durrell J H, Dennis A R, and Cardwell D A 2016 *Supercond. Sci. Technol.* **29** 015010

[25] Namburi D K, Shi Y-H, Zhai W, Dennis A R, Durrell J H and Cardwell D A 2015 *Cryst. Growth Des.* **15** 1472–80

[26] Namburi D K, Shi Y and Cardwell D A 2021 *Supercond. Sci. Technol.* **34** 053002

[27] Houbart M, Fagnard J-F, Dennis A R, Namburi D K, Shi Y-H, Durrell J H and Vanderbemden P 2020 *Supercond. Sci.Technol.* **33** 064003

[28] Quantum design (available at: http://qdusa.com/products/ ppms.html)

[29] Vanderbemden P, Rivas-Murias B, Lovchinov V and Vertruyen B 2010 *Supercond. Sci. Technol.* **253** 012006

[30] Philippe M P, Fagnard J-F, Kirsch S, Xu Z, Dennis A R, Shi Y-H, Cardwell D A, Vanderheyden B and Vanderbemden P 2014 *Physica* C **502** 20–30

[31] Lousberg G P, Fagnard J-F, Chaud X, Ausloos M, Vanderbemden P and Vanderheyden B 2010 *Supercond. Sci. Technol.* **24** 035008

[32] Philippe M P, Fagnard J F, Wéra L, Morita M, Nariki S, Teshima H, Caps H, Vanderheyden B and Vanderbemden P 2016 *J. Phys.: Conf. Ser.* **695** 012003

[33] Fagnard J-F, Morita M, Nariki S, Teshima H, Caps H, Vanderheyden B and Vanderbemden P 2016 *Supercond. Sci. Technol.* **29**

[34] AC measurement system (ACMS) option user's manual (available at: https://web.njit.edu/tyson/PPMS_Documents/PPMS_Manual/1084-100)

[35] Life-HTS (available at: www.life-hts.uliege.be/)

Published in : Supercond. Sci. Technol (2024), vol. 37, 16pp
DOI: 10.1088/1361-6668/ad68d1
Status : Postprint (Author's version)

[36] Dular J, Berger K, Geuzaine C and Vanderheyden B 2022 *IEEE Trans. Magn.* **58** 8205204

[37] Houbart M, Fagnard J-F, Dular J, Dennis A R, Namburi D K, Durrell J H, Geuzaine C, Vanderheyden B and Vanderbemden P 2023 *Supercond. Sci. Technol.* **38** 115012

[38] Yamazaki K 1997 *Electr. Eng. Japan* **118** 111–20

[39] Leconte V 2008 *The Finite Element Method for Electromagnetic Modeling* (Gérard Meunier)

[40] Zhang X, Zhong Z, Geng J, Shen B, Ma J, Li C, Zhang H, Dong Q and Coombs T 2004 *J. Supercond. Novel Magn.* **31** 3847–54

[41] Yamasaki H and Mawatari Y 2000 *Supercond. Sci. Technol.* **13** 202–8

[42] Johansen T H, Koblischka M R, Bratsberg H and Hetland P O 1997 *Phys. Rev.* B **56** 11273–8

[43] Zeldov E, Amer N M, Gupta A, McElfresh M W and Gambino R J 1990 *Appl. Phys. Lett.* **56** 680–2

[44] Sun J Z, Eom C B, Lairson B, Bravman J C and Geballe T H 1991 *Phys. Rev.* B **43** 3002–8

[45] Cardwell D A *et al* 2004 *Physica* C **412–414** 623–2

[46] Koblischka M R, Van Dalen A J J, Higuchi T, Sawada K, Yoo S I and Murakami M 1996 *Phys. Rev.* B **54** R6893

[47] Jirsa M, Pust L and Dlouhy D 1997 *Phys. Rev.* B **55** 3276–84

[48] Abulafia Y *et al* 1996 *Phys. Rev. Lett.* **77** 1596–9

[49] Zhukov A A, Kupfer H, Perkins G, Cohen L F, Caplin A D, Klestov S A, Claus H, Voronkova V I, Wolf T and Wuhl H 1995 *Phys. Rev.* B **51** 12704–14

[50] Civale L, Marwick A D, Worthington T K, Kirk M A, Thompson J R, Krusin-Elbaum L, Sun Y, Clem J R and Holtzberg F 1991 *Phys. Rev. Lett.* **67** 648–51

[51] Vanderbemden P, Hong Z, Coombs T A, Ausloos M, Hari Babu N, Cardwell D A and Campbell A M 2007 *Supercond. Sci. Technol.* **20** S174–83

[52] Martel S *et al* 2007 *Appl. Phys. Lett.* **90** 114105

[53] Li N *et al* 2019 *Ann. Biomed. Eng.* **47** 2402–15

[54] Li N *et al* 2022 *IEEE Trans. Biomed. Eng.* **69** 2616–27

[55] Mathieu J-B and Martel S 2007 *Biomed. Microdevices* **9** 801–8

[56] Mathieu J-B, Beaudoin G and Martel S 2006 *IEEE Trans. Biomed. Eng.* **53** 292–9

[57] Felfoul O, Becker A T, Fagogenis G and Dupont P E 2016 *Sci. Rep.* **6** 33567

[58] Houbart M, Fagnard J-F, Dular J, Dennis A R, Namburi D K, Durrell J H, Geuzaine C, Vanderheyden B and Vanderbemden P 2022 *Supercond. Sci. Technol.* **35** 064005

[59] Hara T, Tanaka T, Kitamura H, Bizen T, Maréchal X, Seike T, Kohda T and Matsuura Y 2004 *Phys. Rev. Spec. Top. Accel. Beams* **7** 050702

[60] Diez-Jimenez E, Perez-Diaz J L, Ferdeghini C, Canepa F, Bernini C, Cristache C, Sanchez-Garcia-Casarrubios J, Valiente Blanco I, Ruiz-Navas E M and MartinezRojas J A 2018 *J. Magn. Magn. Mater.* **451** 549–53

[61] Diez-Jimenez E, Perez-Diaz J L, Canepa F and Ferdeghini C 2012 *J. Appl. Phys.* **112** 063918